Infinite Science Publishing

Research Article

Imaging Characterization of MPI Tracers Employing Offset Measurements in a two Dimensional Magnetic Particle Spectrometer

Daniel Schmidt[a,*] · Matthias Graeser[b] · Anselm von Gladiss[b] · Thorsten M. Buzug[b] · Uwe Steinhoff[a]

[a]Physikalisch-Technische Bundesanstalt, Berlin, Germany
[b]Institute of Medical Engineering, Universität zu Lübeck, Lübeck, Germany
*Corresponding author, email: daniel.schmidt@ptb.de

Abstract

We developed a method to characterize the imaging performance of MPI tracers from virtual MPI measurements that can be synthesized using measurement data from a Magnetic Particle Spectrometer (MPS) at different static magnetic field offsets. MPI system functions were obtained from measurements on a FeraSpin™ R (nanoPET GmbH, Berlin) sample in a 2D MPS comprising two excitation coils and two receive coils. Software phantoms of spatial MPI tracer distributions with different sizes and shapes were constructed. With the measured MPI system function, a synthetic MPI measurement of the software phantoms was simulated. By adding noise to the virtual MPI data, the detection limit of each harmonic in dependence of the noise level was obtained. An MPI reconstruction of the virtual tracer distribution was performed using the virtual MPI data as input. With this method we found the highest tolerable noise level at which it was still possible to distinguish the objects in the phantom. These findings were compared to predictions based on the frequency components that were used in the reconstruction process. This method provides a valuable link between pure spectroscopic characterization and time consuming MPI phantom experiments.

I. Introduction

The search for highly performant MPI tracers is one of the top priorities in the development process of MPI. It is not sufficient to just synthesize MPI tracers with a large magnetic moment. To obtain a strong signal, the magnetic moments also have to quickly realign to the oscillating field by either Brownian or Néel relaxation. This trade-off between size and relaxation dynamics has already been addressed by several groups [1–3]. Since it is not possible to perform phantom experiments for every newly synthesized potential tracer material, Magnetic Particle Spectroscopy (MPS) has been established as a fast and straightforward method for tracer characterization. MPS spectra with high amplitudes (normalized to the iron content) indicate the possibility of achieving a good signal-to-noise ratio (SNR) with a minimal amount of injected MNP.

Recently, we introduced an additional method for the characterization of MPI tracers that combines the measurement speed of MPS and the application-oriented approach of MPI phantom measurements [4]. This method is based on the hybrid system function, which has already been employed to reconstruct MPI measure-

ment data [5, 6]. In this approach, we utilized an MPS equipped with an additional static offset magnet and measured the 1D system function by applying offset fields between the zero field and the drive field amplitude. Employing this data, we generated virtual MPI signals of phantoms and reconstructed them to obtain the resolution limit. The main advantage of this method is the evaluation of the imaging performance directly in the images, which is not possible from the evaluation of single MPS spectra. However, this method could so far only be tested with one-dimensional excitation, therefore lacking the mixed frequencies that occur in 2D and 3D MPI with drive fields with different frequencies. To overcome this limitation, we applied the MPS-based imaging characterization on measurement data from a newly built 2D MPS setup [7], thereby including the mixed frequencies in the reconstruction process as well as in our prediction of the spatial resolution. This is an integral step towards predicting the MPI resolution of different tracers.

II. Method

In our previous 1D approach we discretized the field gradient into static offset steps with increments of $B_{Incr} = 0.25$ mT. By switching through the offsets and measuring the MPS spectra at each static offset, we gradually obtained the 1D system function.

For a drive field of $B_{Drive} = 12$ mT, the offset field was shifted between $B_{off} = [0$ mT, $+12$ mT$]$. After mirroring the results for negative fields, this leads to $N = 97$ spectra spanning the 1D system function. These measurements, each with a different offset field, have been used to generate synthetic MPI data s_{MPI} of a defined 1D phantom by weighting the normalized spectra S_n/A with an iron mass m_n at location n and superposing these spectra. Additionally, noise W may be added to test the resolution under different noise conditions.

$$s_{MPI} = \sum_{n=1}^{N} m_n \frac{S_n}{A} + W \qquad (1)$$

The signal generation in 2D that is presented here differs from the signal generation in 1D. From the drive field amplitude and the offset field increment, the number of simulation points in the field of view is determined to be 97 in each direction. Thus, $N = 97^2 = 9409$ spectra were considered, since all offset combinations of both the x-axis and the y-axis have to be taken into account. Also, mixed frequencies are taken into account, resulting from the simultaneous excitation with two different frequencies in x- and y-direction.

For the 2D experiments, we employed the 2D MPS built at the Institute of Medical Engineering, Universität zu Lübeck, which consists of two transmit and receive coils. With such a system, it is possible to explore the

influence of particle excitation in two dimensions with or without magnetic offset fields.

To obtain an MPI system function of the commercially available MPI tracer FeraSpin™ R, we measured the positive quadrant of the overall field of view. The measurement consisted of 49×49 spectra with the offset field strengths $B_{off,x} = [0$ mT, $+12$ mT$]$ and $B_{off,y} = [0$ mT, $+12$ mT$]$ (Fig. 1) corresponding to the drive field of $B_{Drive} = 12$ mT for both x- and y-direction. The drive field frequencies $f_x = 25.25$ kHz and $f_y = 26.04$ kHz were those of a typical MPI scanner. Due to the symmetry, we mirrored the measured data to the three other quadrants [8]. Additionally, for the reconstruction of the virtual tracer distribution, we measured a reduced system function with 13×13 2D offset steps with $B_{off,x,y} = [0$ mT, $+12$ mT$]$ and $B_{Incr} = 1$ mT which resulted in 25×25 MPI spectra after mirroring as described above. In order to map the measured spectra to a virtual field of view, a value for the gradient field has to be assumed. Here, we used a gradient field strength of $G_{x,y} = 1.25$ T/m which corresponds to a field of view of the size 19.2 mm×19.2 mm. Given the number of measured spectra, this resulted in increments of 0.2 mm for the full system function and 0.77 mm for the reduced one. Thus, we could only simulate phantoms with larger dimensions spanning several voxels of 0.77 mm side length. In each measurement cycle of $t = 253$ ms the full area MPI signal was 200 times averaged.
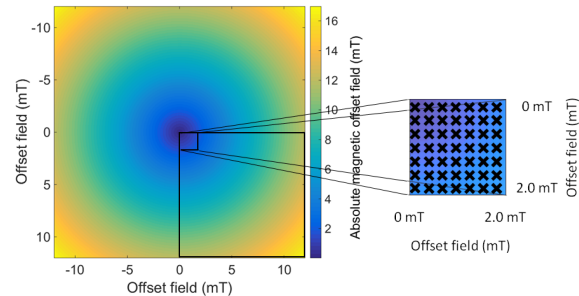
Figure 1: Division of the spatial dependent offset in 0.25 mT increments. Large image: The frame depicts the measured quadrant with offset fields between 0 mT and 12 mT in x- and y-direction; Small image: Magnification of the measurement grid. Each cross represents a simulation point where the MPS spectrum was measured for a pair of offset amplitudes.

We then defined 2D software phantoms consisting of two rectangular distributions with a distance to each other corresponding to their edge length [9]. We assumed a layer thickness corresponding to the edge length, resulting in cubic objects (Fig. 2, left). The edge length of these objects varied between 2.4 mm and 4 mm. The iron concentration was assumed to be homogeneous throughout the phantom at $c = 50$ mmol/L. In addition to the cubic-shaped phantoms, we also defined phantoms with sinusoidally shaped outer boundaries (Fig. 2, right). Using

these phantoms, we generated the respective virtual MPI data by applying (1).
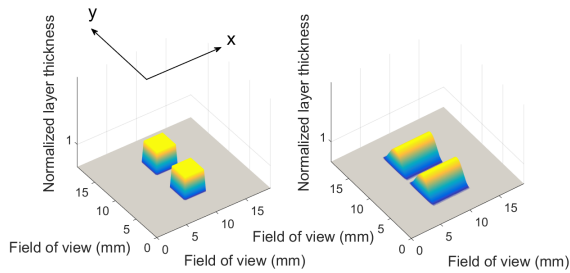
Figure 2: Left: Cubic-shaped phantom; Right: Sinusoidally shaped phantom.

The non-negative Kaczmarz algorithm was used for reconstruction with a regularization factor between $\lambda = 0.01$ and $\lambda = 0.05$. We then determined the maximum noise level where the phantoms could still be distinguished. For this, we gradually raised added Gaussian noise to the virtual MPI signal and performed a reconstruction of the tracer distribution, taking into account only frequency components above the resulting noise level. Thus, we found the noise level where the two phantoms could just be distinguished from each other in the reconstructed MPI distribution.

We compared our findings with an analytical method to estimate the resolution R at a given SNR level, as it has been derived in [9]. Note that we defined the resolution as the distance between two object centers, not as the distance between the edges of two objects (like it was done in [9]), which seems more reasonable when using sinusoidally shaped phantoms. We assumed the highest available spatial frequency component to be responsible for the resolution limit. We experimentally derived the respective spatial frequency from the frequency components above noise level and calculated the resolution with the relation

$$R = \frac{l_{\mathrm{FOV}}}{F_{\max}} = \frac{1}{f_{\max}} \tag{2}$$

where l_{FOV} is the size of the field of view and $F_{\max}$ is the unitless maximum number of spatial periods over the field of view found in the frequency components above noise. The resolution R corresponds to the inverse of the maximum spatial frequency $f_{\max}$ (measured in line pairs per mm). It should be noted here that due to the 2D character, the spatial frequencies might differ for the x- and y-directions in one frequency component. Since the virtual objects in our phantoms were assembled in the y-direction, we only analyzed y-directed spatial frequencies.

We compared the resolution derived from the spatial frequencies at resolution limit with the distance between the object centers for both cubic and sinusoidal tracer distribution.

III. Results

In Fig. 3, the cubic phantoms (left) can be seen in comparison to the reconstructed images (middle) for phantom sizes of 2.4 mm, 3.2 mm and 4.0 mm or 4.8 mm, 6.4 mm and 8.0 mm distances between the phantom centers. The noise level was the highest possible to still resolve two separate objects. Here we were able to raise the maximum tolerated noise levels to $W = 3E-10\,\mathrm{Am}^2$ for 2.4 mm, $W = 1E-9\,\mathrm{Am}^2$ for 3.2 mm and $W = 6E-9\,\mathrm{Am}^2$ for 4.0 mm for cubic phantoms. For the sinusoidally shaped phantoms, the tracers were spread over more voxels than for the cubic phantoms, where the tracers were concentrated on few voxels. Furthermore, the iron content was lower than for the cubic phantoms due to the lower total volume, which resulted in a lower SNR. Thus, the tolerated noise level was slightly decreased for the sinusoidally shaped phantoms.

For the cubic and sinusoidal phantoms, we analyzed the frequency components above the noise level, which were used for reconstruction. From the component with the highest spatial frequency (Fig. 3, right) we used (2) to derive the resolution and compared these calculated values to the distance between the object centers.
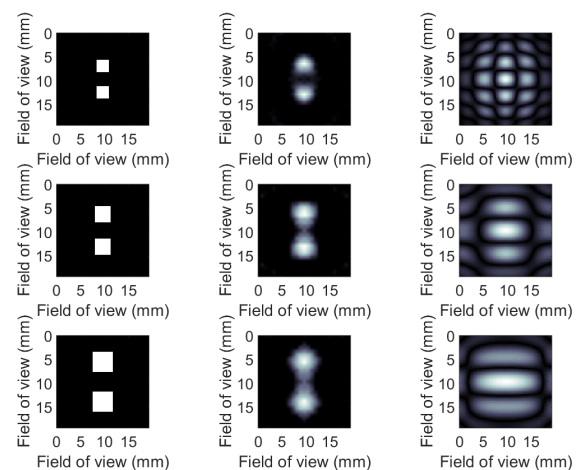
Figure 3: Left: Cubic phantom of the sizes 2.4 mm, 3.2 mm and 4.0 mm; Middle: Reconstructed image at highest tolerated noise level; Right: Absolute values of the spatially resolved amplitude of the frequency component with highest spatial frequency in vertical direction.

As can be seen, the vertical spatial frequency changes for each phantom from a very tight grid for a 2.4 mm edge length, which is needed to ensure the high resolution to a relatively coarse grid for 4.0 mm. As a practical example the resolution for the 2.4 mm (or 4.8 mm center distance) phantom can be calculated by applying (2) with $l_{\mathrm{FOV}} = 19.2\,\mathrm{mm}$ and $F_{\max} = 3.5$ (seven extrema indicating 3.5 periods) to $R = 19.2\,\mathrm{mm}/3.5 = 5.5\,\mathrm{mm}$. Note that in Fig. 3 the absolute values of the amplitudes are depicted, therefore only the white dots are counted as

extrema.

Tab. 1 depicts a comparison between the actual distance between the objects and the respective resolution derived from the maximum spatial frequencies in Fig. 3 at the resolution limit. It can be seen that the prediction based on the cubic phantoms tends to slightly underestimate the potential resolution. Using sinusoidal phantoms, there is no such trend. The difference between the predictions for the cubic and sinusoidal phantoms is based on the different amount of iron present in the different phantom shapes as explained above, thus leading to a different number of frequency components used for reconstruction.

Table 1: Predicted resolution in comparison to actual distance between phantom centers

Center Distance	Prediction (Cubic Phantom)	Prediction (Sinusoidal Phantom)
4.8 mm	5.5 mm	4.3 mm
6.4 mm	7.7 mm	6.4 mm
8.0 mm	8.5 mm	8.5 mm

Overall, the predictions for sinusoidally shaped particle distributions exhibited deviations of 12% or less in comparison to the defined center distance while the deviations for cubic phantoms ranged between 6% and 17%.

IV. Conclusion

In this work, we applied an imaging characterization technique to obtain the maximum tolerated noise level at which a certain spatial MPI resolution could still be reached. For that, we used two-dimensional phantoms, which so far has only been reported for the one-dimensional case. We compared the distance between virtual objects and predicted resolutions based on the resolvable spatial frequencies used for reconstruction. While it was sufficient to evaluate the pure harmonics for 1D, we have now taken the mixed frequencies of excitation into account as well. The prediction of the spatial resolution in two dimensions worked well with slight deviations for cubic phantoms and accurate predictions for sinusoidal phantoms.

It will still be necessary to compare the results obtained here to actual MPI experiments, especially the comparison between tolerated noise level (or SNRs) in MPI and our MPS based predictions. Another part of this comparison will be to evaluate if both systems yield the same spectra at the respective offset fields, as this is important for matching results in both experiments.

Overall, this method provides a valuable link between pure spectroscopic measurement and time-consuming phantom measurements in an actual MPI setup as it yields results that are more end-user oriented.

References

[1] R. M. Ferguson, K. R. Minard, and K. M. Krishnan. Optimization of nanoparticle core size for magnetic particle imaging. *J. Magn. Magn. Mater.*, 321(10):1548–1551, 2009. doi:10.1016/j.jmmm.2009.02.083.

[2] D. Eberbeck, F. Wiekhorst, S. Wagner, and L. Trahms. How the size distribution of magnetic nanoparticles determines their magnetic particle imaging performance. *Appl. Phys. Lett.*, 98(18):182502, 2011. doi:10.1063/1.3586776.

[3] F. Ludwig, D. Eberbeck, N. Löwa, U. Steinhoff, T. Wawrzik, M. Schilling, and L. Trahms. Characterization of magnetic nanoparticle systems with respect to their magnetic particle imaging performance. *Biomed. Tech. / Biomed. Eng.*, 58(6):535–545, 2013. doi:10.1515/bmt-2013-0013.

[4] D. Schmidt, F. Palmetshofer, D. Heinke, O. Posth, and U. Steinhoff. Characterizing the imaging peformance of magnetic tracers by magnetic particle spectroscopy in an offset field. In *International Workshop on Magnetic Particle Imaging (IWMPI)*, 2015. doi:10.1109/iwmpi.2015.7107006.

[5] M. Graeser, M. Gruettner, S. Biederer, H. Wojtczyk, W. Tenner, T. F. Sattel, B. Gleich, J. Borgert, T. Knopp, and T. M. Buzug. Determination of a 1d-mpi-system-function using a magnetic particle spectroscope. In *Jahrestagung der Deutschen Gesellschaft für Biomedizinische Technik*, volume 56, 2011.

[6] M. Gruettner, M. Graeser, S. Biederer, T. F. Sattel, H. Wojtczyk, W. Tenner, T. Knopp, B. Gleich, J. Borgert, and T. M. Buzug. 1d-image reconstruction for magnetic particle imaging using a hybrid system function. In *IEEE Nuclear Science Symposium and Medical Imaging Conference (NSS/MIC)*, pages 2545–2548, 2011. doi:10.1109/NSSMIC.2011.6152687.

[7] M. Graeser, M. Ahlborg, A. Behrends, K. Bente, G. Bringout, C. Debbeler, A. von Gladiss, K. Graefe, C. Kaethner, S. Kaufmann, K. Lüdtke-Buzug, H. Medimagh, J. Stelzner, M. Weber, and T. M. Buzug. A device for measuring the trajectory dependent magnetic particle performance for mpi. In *International Workshop on Magnetic Particle Imaging (IWMPI)*, 2015. doi:10.1109/iwmpi.2015.7107078.

[8] A. Weber and T. Knopp. Symmetries of the 2d magnetic particle imaging system matrix. *Phys. Med. Biol.*, 60(10):4033, 2015. doi:10.1088/0031-9155/60/10/4033.

[9] T. Knopp, S. Biederer, T. F. Sattel, M. Erbe, and T. M. Buzug. Prediction of the spatial resolution of magnetic particle imaging using the modulation transfer function of the imaging process. *IEEE Trans. Med. Imag.*, 30(6):1284–1292, 2011. doi:10.1109/tmi.2011.2113188.